ADVANCED ENGINEERING MATERIALS
www.aem-journal.com

Sputtering and Characterization of MAX-Phase Forming Cr–Al–C and Ti–Al–C Coatings and Their Application on γ-Based Titanium Aluminides

Nadine Laska, Peter-Philipp Bauer, Oliver Helle, and Frederic Kreps*

MAX-phases are of increasing interest as coating material for high temperature applications due to their unique metallic as well as ceramic properties. Herein, the deposition of Cr_2AlC and Ti_3AlC_2 or Ti_2AlC MAX-phase forming coatings by magnetron sputtering is demonstrated. Using pure elemental targets, the manufacturing with a coating thickness of above 7 µm is established. The MAX-phase forming coatings are characterized by high-temperature X-ray diffraction (HT-XRD) measurements and provide a good oxidation behavior due to the development of protective thermally grown oxide layers. The performance of the MAX-phases is strongly depended on the substrate material and the accompanying interdiffusion processes. Therefore, the Ti–Al–C coating is favored for TiAl alloys due to the thermodynamic stability of the Ti_2AlC MAX phase in particular in the presence of the γ-TiAl phase. An excellent oxidation behavior is confirmed up to 300 h at 850 °C due to the development of an alumina layer above a homogenous Ti_2AlC phase coating. The Cr_2AlC MAX-phase coating degrades after 100 h at 800 °C due to interdiffusion processes between coating and substrate and the accompanying development of carbides and nitride phases. Nevertheless, the oxidation resistance of the Cr–Al–C-coated TiAl alloy is given by the formation of the Ti_2AlC MAX-phase.

1. Introduction

MAX-phases $M_{n+1}AX_n$ ($n = 1$–4) are a class of ternary nanolaminates, where M is an early transition metal, A is an A-group element, and X is nitrogen or carbon. Due to the strong M—X bond and relatively weak M—A bond, the MAX-phases exhibit a unique combination of typical ceramic properties (e.g., low density, high melting point, and high strength) and typical metallic properties (e.g., good thermal and electrical conductivity, easy machinability, excellent thermal shock resistance, and damage tolerance).[1–4] High oxidation resistance has been observed in MAX-phases due to the development of a protective thermally grown oxide (TGO) layer for the alumina formers $Ti_{n+1}AlX_n$ (with X = C or N) and Cr_2AlC as well on the silica former Ti_3SiC_2.[5] The implementation of these MAX-phases as coating material for high temperature applications is a promising approach due to their outstanding oxidation performance.[6–10] A further advantage of these MAX-phase materials is the crack healing ability of the alumina forming MAX-phases.[11,12] Previous work, e.g., by Berger et al. has looked at this "self-healing" effect on coated and afterward artificially precracked samples during high temperature exposure in air. The crack in the MAX-phase coatings fills with oxide of predominantly alumina to form a covering protection layer on the crack flanks.[13]

The successful synthesis of these thin films by the utilization of several coating techniques, e.g., magnetron sputtering or plasma spraying and the application as protective layers for metallic high temperature alloys has been published in numerous previous work.[8,14–17]

The alumina forming MAX-phases are in particularly promising as protective coatings for γ-TiAl-based titanium aluminide alloys. Most previously applied coating materials on TiAl alloys were based on Ti–Al–Cr,[18–20] Al–Ti,[21,22] or Al–Si.[23,24] While they provide excellent oxidation protection, they finally degrade due to an Al depletion in the coating material, which consequently results in the formation of nonprotective oxides such as TiO_2. Combining a TiAl substrate with a MAX-phase forming coating is a promising approach, as the substrate material may serve as an Al reservoir, resupplying the coating by outward diffusion of Al. Moreover, protective MAX-phase-based layers could provide an advanced mechanical behavior of such coated engine components. In comparison with the brittle intermetallic phases which are usually present in other protective alumina forming coatings,[25,26] MAX-phases offer a higher fatigue resistance[27] as well as a promising wear resistance.[28] In particular, the Ti-based MAX-phases $Ti_{n+1}AlX_n$ (with X = C or N) are suitable for titanium aluminides because of their similar coefficients of thermal expansion (CTE) with 8–9 × 10^{-6} (K^{-1}) for Ti_2AlC and

N. Laska, P.-P. Bauer, O. Helle, F. Kreps
German Aerospace Center
Linder Hoehe
Cologne 51147, Germany
E-mail: nadine.laska@dlr.de

The ORCID identification number(s) for the author(s) of this article can be found under https://doi.org/10.1002/adem.202100722.

DOI: 10.1002/adem.202100722

Ti_2AlN and about 10×10^{-6} (K^{-1}) for TiAl-based alloys,[29,30] whereas the Cr_2AlC MAX phase with a CTE of about 13×10^{-6} (K^{-1}) is more appropriate for Ni-based alloys.[31]

Previous work by Abdulkadhim et al. has shown that the formation of the hexagonal Cr_2AlC MAX-phase coatings already occurs at 600 °C,[32] whereas the Ti-based MAX-phases are formed at a higher temperature of about 800 °C.[33] Therefore, the Cr_2AlC MAX-phase could be more suitable for TiAl alloys, because it requires less temperature for its crystallization heat treatment, which in turn has fewer negative influences on the mechanical properties of the substrate material.

The oxidation behavior of the Cr_2AlC MAX-phase on a Ti-based alloy has been already tested by Wang et al.[34] Oxidation tests up to 800 °C revealed an improvement of the oxidation behavior of the Ti-alloy Ti6242 coated with Cr_2AlC MAX-phase layer due to the development of a continuous and dense Al-rich TGO. Moreover, the Cr_2AlC coating itself acted as a diffusion barrier for the inward diffusion of oxygen. Therefore, the well-known oxygen embrittlement of TiAl-based alloys caused by the accompanying changes in the microstructure could probably be prevented.[35] In this work MAX-phase forming Ti–Al–C and Cr–Al–C coatings were applied on alumina substrates as well as on the commercial alloy TiAl48-2-2. The performance of these coatings as protective layers was examined during exposure at service temperatures of conventional TiAl alloys in aircraft engines.

2. Experimental Section

The MAX-phase-based coatings presented in this study were produced by DC magnetron sputtering using a multisource sputter coater (IMPAX 1000 HT system by SVS Vacuum Coating Technologies, Karlstadt, Germany). The Cr–Al–C as well as the Ti–Al–C coatings were deposited using four pure elemental target materials, one chromium or titanium, one aluminum and, because of the low sputter rate of carbon, two carbon sources. No additional heating was applied during the sputtering process, the obtained substrate temperature was self-adjusted due to the target power. Prior to coating deposition, an Ar-plasma etching process for surface cleaning using a bias voltage of 500 V and a frequency of 100 kHz was carried out for 15 min. During the deposition process with a total duration of 7 h, the flat substrate specimens were threefold rotated to provide a homogenous all-around coating deposition. The used sputter parameters are shown in **Table 1**.

Two different substrate materials were used as flat specimens. For preliminary experiments and optimization of the sputter process flat rectangular α-Al_2O_3 samples with a purity of 99.6% by Quick-Ohm Küpper & Co. GmbH were used, whereas samples made of the γ-based TiAl alloy TiAl48-2-2 (48Ti–48Al–2Nb–2Cr in at%) supplied by GfE–Gesellschaft für Elektrometallurgie, Nuremberg, Germany, were used for all oxidation and interdiffusion experiments. From the extruded and annealed TiAl48-2-2 rods, disc-shaped specimens with 15 mm diameter and 1 mm thickness were machined. The surfaces of the TiAl specimens were ground using SiC emery paper up to 2500 grit and subsequently ultrasonically cleaned in ethanol prior to the coating deposition process.

Table 1. Parameters during DC magnetron sputtering of the Cr–Al–C and Ti–Al–C coatings.

Coating	Cr target [kW]	Ti target [kW]	Al target [kW]	C target [kW][a)]	p [bar]	T [°C]	Ar [sccm]
Cr-Al-C	0.7	–	0.5	1.2	5.2×10^{-3}	255	300
Ti-Al-C	–	1.7	0.6	1.2	5.7×10^{-3}	194	

[a)]Utilization of two C-targets on opposite sides.

Cross sections of the coated specimens were metallographically prepared and analyzed with scanning electron microscopy (SEM) using a DSM Ultra 55, Carl Zeiss NTS, Wetzlar, Germany equipped with energy-dispersive X-ray spectroscopy (EDS) by Aztec, Oxford Instruments, Abingdon, UK. All SEM images were taken with a secondary electron detector. The EDS measurements were carried out at 15 kV using a working distance of 8.5 mm.

In addition, wavelength-dispersive spectrometry (WDS) with adequate standards that provide a higher accuracy was used. Therefore, the quantitative analysis of the C content in the as-coated states was done with a Thermo Fisher Scientific Pathfinder Mountaineer system combining an ultradry energy-dispersive X-ray spectrometer and a MagnaRay wavelength-dispersive X-ray spectrometer. Both devices are equipped at a FEI Helios NanoLab 600i dualbeam microscope (FIB-SEM). To guarantee an optimal WDS quantification, certified MAC standards for carbon (highest purity), aluminum (99.9990 wt% purity), chromium (99.996 wt% purity), and titanium (99.9900 wt% purity) were used. The WDS-crystals for carbon was NiC80 and PET for the other elements. Each standard setup and measurement was done with 10 and 15 keV to optimize the accuracy of the results for all samples.

For in situ investigation of the evolution of phases, high-temperature X-ray diffraction (HT-XRD) measurements were carried out using Cu Kα radiation with a step size of 0.1° and a 2θ range from 10° to 80° in a D8 Advance diffractometer by Bruker equipped with a high temperature oven chamber HTK 1200 N by Anton Paar. For the HT-XRD measurements, temperature range from 500 to 1000 °C with 100 °C steps and a holding time of 45 min prior to each 15 min measurement was chosen to obtain a total holding time of 1 h for each measurement. The XRD measurements were carried out in laboratory air with a heating rate of 5 K min^{-1}. Moreover, a Bragg–Brentano geometry was used for HT-XRD as well as for the subsequent conventional X-ray diffraction (XRD) measurements at room temperature. Moreover, the Bruker AbsorbDX from the DIFFRAC.EVA software was utilized to calculate the angle-dependent maximum signal depths.

Isothermal oxidation tests of the coated TiAl48-2-2 samples were carried out in laboratory air in a box furnace N11/H by Nabertherm GmbH. The Cr–Al–C coating on the TiAl48-2-2 alloy was exposed to 800 °C for 100 h, whereas the Ti–Al–C coating was tested for 300 h at 850 °C using a heating rate of 5 K min^{-1}.

3. Results

3.1. Characterization of the Magnetron-Sputtered Cr–Al–C Coating

The Cr–Al–C coating deposited by DC magnetron sputtering shows a columnar morphology, a homogeneous elemental

distribution, and a thickness of around 7.25 µm amounting to a deposition rate of 1 µm h^{-1}. An SEM cross section of the as coated Cr–Al–C coating on an Al_2O_3 substrate is shown in **Figure 1**. The columnar coating morphology was expected according to the structural zone model by Thornton[36] as no additional substrate heating, bias voltage or ionization was used. Due to the roughness and surface structure of the alumina substrate, the columnar structure was more pronounced on this substrate material than on TiAl. Using WDS, the composition of the deposited coating was measured to be 49Cr–27Al–24C (at%), which is close to the stoichiometric Cr_2AlC MAX-phase composition. XRD measurements (shown in Figure 1b) at room temperature show that the coating is amorphous while reflections from the Al_2O_3 substrate are visible, indicating that the substrate temperature of 255 °C during deposition is too low to activate any crystallization processes in the coating. This is in agreement with previous investigations by Stelzer et al.,[37] suggesting that a post-heat treatment after deposition is necessary for the formation of the desired hexagonal Cr_2AlC MAX-phase when deposited within this temperature range.

To study the phase formation, in situ HT-XRD measurements were carried out from 500 up to 1000 °C and finally after cooling down at room temperature. The X-ray measurements in 100 °C steps carried out in laboratory air are shown in **Figure 2**.

The results reveal that the crystallization process of the amorphous Cr–Al–C coatings starts at around 500 °C as indicated by the disappearance of the amorphous hill and the appearance of the disordered solid solution $(Cr,Al)_2C_x$, peak at 41.3°, which is in agreement with previous HT-XRD measurements by Abdulkadhim et al.[32] At 600 °C, the distinctive peak of the ordered hexagonal Cr_2AlC MAX-phase at 13.7°[32] can be distinguished from the background. Beginning at 900 °C, additional peaks corresponding to the $Cr_{23}C_6$ phase could be indicated as a result of the Al_2O_3 formation during the heat treatment in air, which in turn led to a depletion of Al in the coating. The formation of α-Al_2O_3 can be confirmed by the peak formed at 25.5° after 45 min at 900 °C. At this angle and the used Bragg–Brentano geometry, the main signal originates from the top 5 µm of the coating. Therefore, the signal corresponds to an oxide phase within this volume. The intensity of the Al_2O_3 peak increases slightly after holding the temperature at 1000 °C,

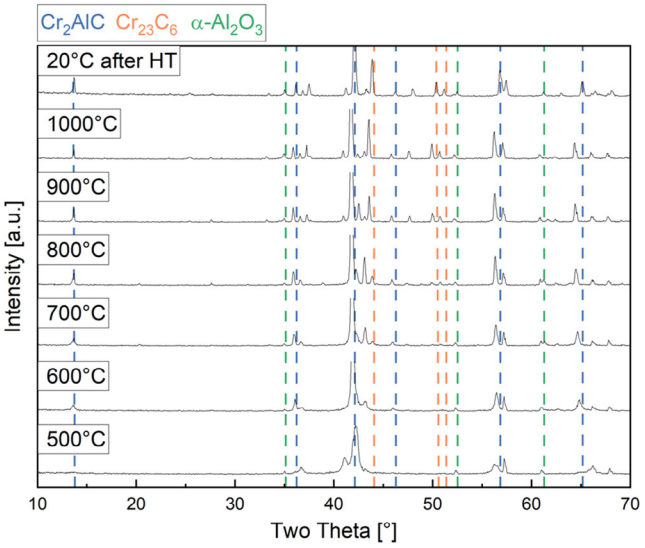

Figure 2. HT-XRD measurements of the Cr–Al–C coating on alumina substrate from 500 to 1000 °C in lab air.

indicating progressing formation of alumina. Moreover, no Cr_2O_3 formation was detected in HT-XRD confirming the preferential alumina formation of the Cr_2AlC MAX-phase.[7] Moreover, a peak shift to lower angles with rising temperature is clearly visible, due to thermal expansion of the lattices. In the final X-ray diffractogram at room temperature, all reflections are located at the specified 2θ angles.

Figure 3 shows the SEM cross section of the Cr–Al–C coating after the HT-XRD measurements up to 1000 °C with the corresponding element mappings and the nominal chemical composition measured by EDS. An about 0.5 µm thick, continuous and dense TGO layer of pure alumina formed on the coating surface. Moreover, the intercolumnar gaps, which were visible directly after the deposition process, were closed due to local internal oxidation of aluminum. The Cr–C phase, which is indicated to be $Cr_{23}Al_6$ by the XRD measurements, is also clearly visible in the SEM cross section and seemed to form preferentially next to the alumina-filled gaps. The chemical composition of the Cr_2AlC

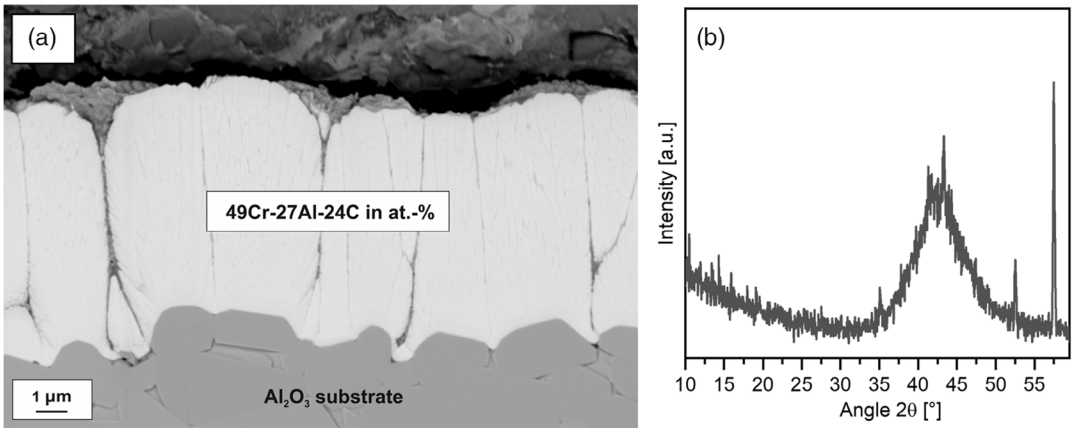

Figure 1. SEM cross section of the Cr_2AlC coating on alumina after deposition using a) magnetron sputtering and b) corresponding XRD pattern.

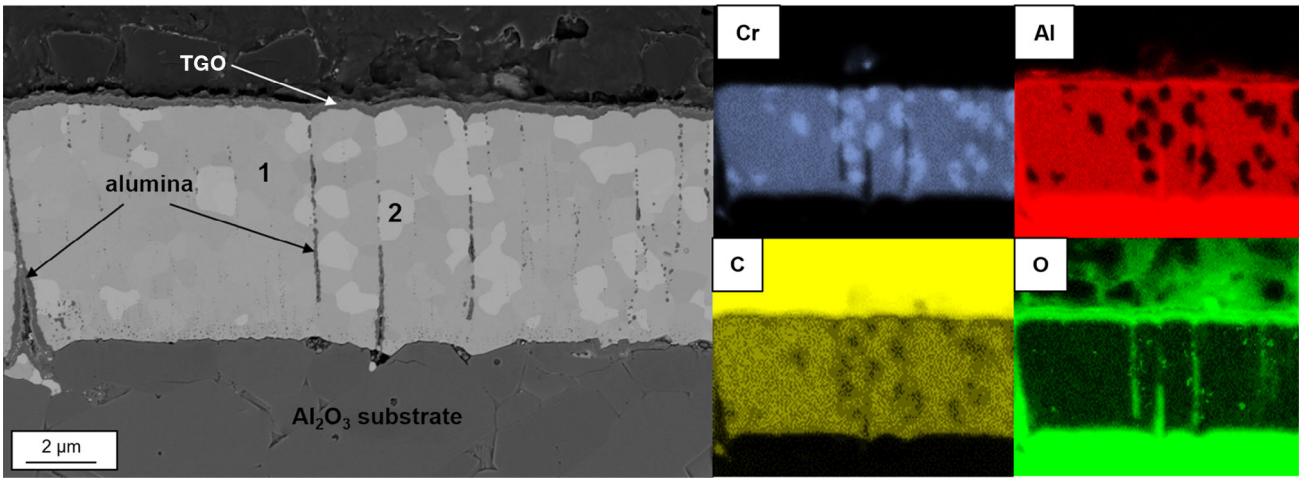

Figure 3. SEM cross section of the Cr–Al–C coating after in situ heat treatment using HT-XRD up to 1000 °C in air with the corresponding EDS element mappings. The composition of the regions 1 and 2 is shown in Table 2.

MAX-phase, as well as that of the Cr–C phase measured by EDS, which is shown in **Table 2**, show a high oxygen content, due to the internal oxidation of alumina in the coating gaps, and the spot size of the EDS measurement points. Considering the Cr–Al ratio in conjunction with the XRD results, the formation of the desired Cr_2AlC MAX-phase could be confirmed.

3.2. Characterization of the Magnetron-Sputtered Ti–Al–C Coating on Alumina

The Ti–Al–C coating deposited by DC magnetron sputtering shows a similar columnar morphology like the Cr–Al–C coating in the as coated state, which is also in agreement with the structural zone model by Thornton.[36] A homogeneous elemental distribution and a coating thickness of around 7.25 µm was measured. The nominal chemical composition of 41Ti–26Al–33C (at%) after the deposition process was also determined by WDS. The cross section of the Ti–Al–C coating in the as-coated state on an Al_2O_3 substrate is shown in **Figure 4**.

The corresponding XRD measurement of the as-coated sample, also shown in Figure 4, confirms the expected amorphous structure of the Ti–Al–C coating. The few sharp reflections originate from the Al_2O_3 substrate.

In situ HT–XRD measurements in air were used to study the phase formations in the Ti–Al–C coating, shown in **Figure 5**. At 500 °C, the amorphous hill disappeared, but below 700 °C no distinguishable peaks other than from the α-Al_2O_3 substrate material could be identified. After 1 h at 700 °C, the XRD results indicate the formation of the ternary MAX-phase Ti_3AlC_2, but also the formation of a solid solution is possible. In addition, the formation of rutile TiO_2 takes place in the same temperature range discernible by the peak at around 27°. The intensity of this peak did not significantly change up to a temperature of 800 °C. However, at 900 °C, the intensities of both, the peak corresponding to TiO_2 at 27° as well as the Al_2O_3 peak at around 25°, increase noticeably. At a higher temperature of 1000 °C, the intensity of both of the oxide reflections only increased slightly. The peaks of the ternary Ti_3AlC_2 MAX-phase changed their intensities above a temperature of 800 °C. In comparison with the Cr–Al–C coating, no reflections of carbides, could be detected by XRD. At 1000 ° C, no significant changes in the X-ray diffractogram were visible anymore. Room temperature measurement that are carried out afterward confirms the achieved equilibrium in the Ti–Al–C coating.

Table 2. Chemical composition of spot 1 (Cr_2AlC) and spot 2 ($Cr_{23}C_6$) shown in Figure 3 in at% as measured by EDS.

Concentration [at%]	Cr	Al	C	O
1 Cr_2AlC MAX-phase	39	18	29	14
2 $Cr_{23}C_6$	49	5	26	20

Figure 6 shows the SEM cross section of the Ti–Al–C coating after the stepwise heat treatment during the HT-XRD measurement up to a temperature of 1000 °C. A continuous and dense TGO of about 1 µm thickness formed on the surface. The TGO consists of two layers, an upper TiO_2 layer of about 200 nm and an underlying Al_2O_3 layer of about 1 µm. Below the TGO, the intercolumnar gaps of the sputter coating closed completely during the HT-XRD measurements and a homogeneous layer of probably the ternary MAX-phase Ti_3AlC_2 was formed. The corresponding chemical compositions by EDS are presented in **Table 3**. Contrary to the Cr–Al–C coating, there were no indications of local internal alumina formation. Moreover, the SEM cross section confirms that no carbides formed in the Ti–Al–C coating or at the interface to the TGO. Due to the oxide formation the Ti–Al–C coating thickness decreased slightly to around 7 µm.

3.3. Application of the Magnetron-Sputtered Cr–Al–C and Ti–Al–C Coating on Commercial γ-Titanium Aluminide Substrate

To determine the potential of these MAX-phase coatings for high temperature applications, the interdiffusion processes between coating and a TiAl alloy were investigated during high temperature exposure. The following oxidation tests were carried out by a

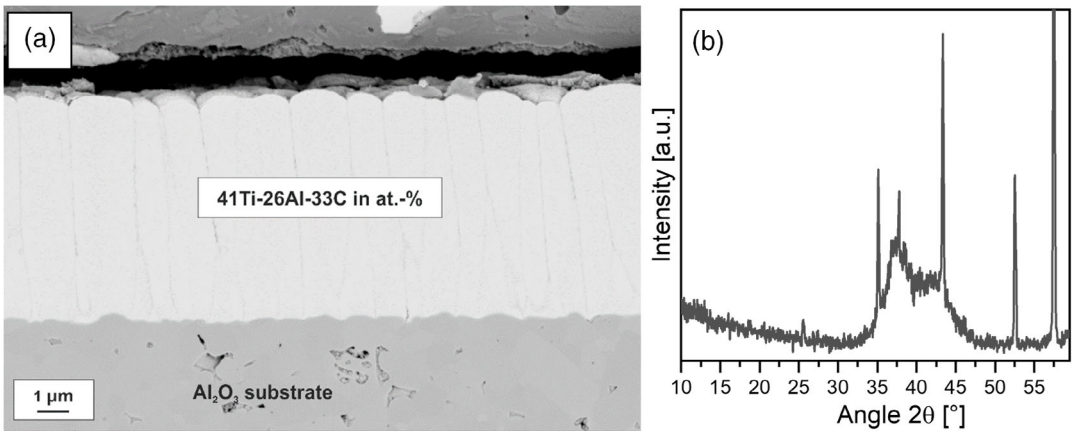

Figure 4. SEM cross section of the Ti_2AlC coating after deposition using a) magnetron sputtering and b) corresponding XRD pattern.

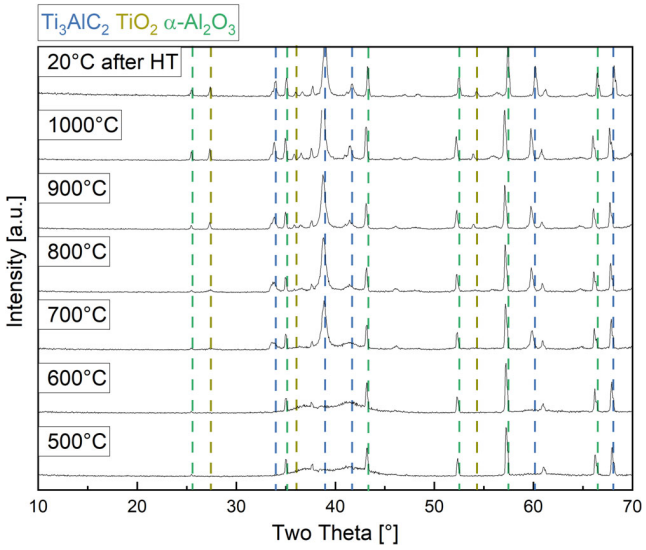

Figure 5. HT-XRD measurements of the Ti–Al–C coating in lab air from 500 to 1000 °C.

direct exposure of the amorphous coating to a high temperature oxidizing environment without any postcoating heat treatment.

3.3.1. Application of the Cr–Al–C Coating on the TiAl48-2-2 Alloy

Figure 7 shows the SEM cross section of the Cr–Al–C coating applied on the TiAl48-2-2 alloy after isothermal exposure for 100 h to 800 °C in laboratory air. The chemical composition measured by EDS in at% are shown in **Table 4**.

The Cr–Al–C coating developed the desired Cr_2AlC MAX-phase as well as the Cr_7C_3 phase. The initially formed columnar gaps of the sputter coating were filled by alumina. Close to the TiAl-based substrate interface a nitrogen content up to 44 at% was measured, due to the formation of chromium nitride. The chromium carbide and especially the lower nitride grains are surrounded by a thin alumina layer. On the coating surface, no TGO layer could be observed. Instead of a TGO layer on the coating surface, the formation of a closed pure alumina layer is visible at the coating–substrate interface. Below the Cr–Al–C coating, an interdiffusion zone (IDZ) developed in the TiAl substrate with an overall thickness of >6 µm. The chemical composition of the upper part of the IDZ (≈2 µm)

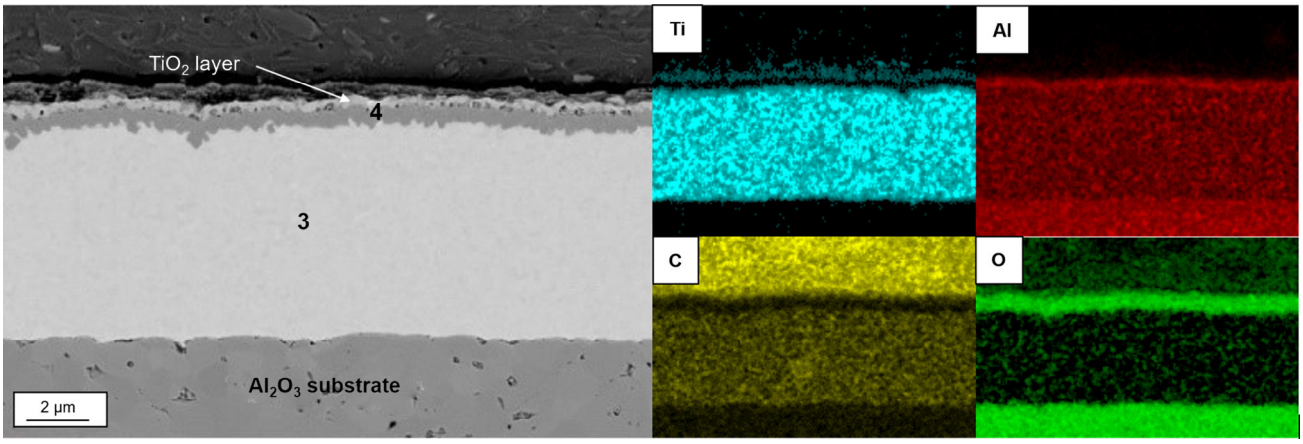

Figure 6. Cross section of the Ti–Al–C coating after in situ heat treatment using HT-XRD up to 1000 °C with corresponding EDS element mappings.

Table 3. Chemical composition of spot 3 and spot 4 shown in Figure 6, measured by EDS in at%.

Concentration [at%]	Ti	Al	C	O
3 Ti_3AlC_2 MAX-phase	48	21	31	–
4 TGO layer of Al_2O_3	3	31	–	66

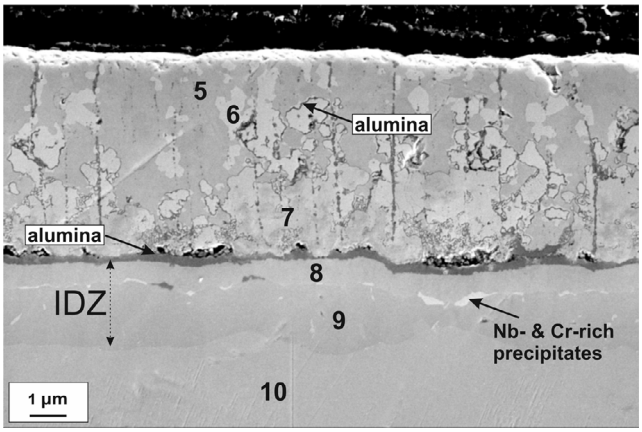

Figure 7. SEM cross section of the Cr–Al–C coating on TiAl48-2-2 after 100 h of isothermal exposure to 800 °C in air.

Table 4. Nominal chemical composition of the spots 5–10 shown in Figure 7, measured by EDS in at%.

Concentration [at%]	Cr	Al	C	Ti	[Nb]	[N]
5 Cr_2AlC MAX-phase	48	25	27	–	–	–
6 Cr_7C_3	65	3	31	1	–	–
7 CrN	49	6	–	1	–	44
8 Ti_2AlC MAX-phase	1	27	24	46	2	–
9 $TiAl_2$	2	64	–	33	1	–
10 TiAl48-2-2	2	48	–	48	2	–

near the coating interface matches with the binary Ti_2AlC MAX-phase, whereas an underlaying Al-rich TiAl layer of probably $TiAl_2$ (≈4 µm) is visible. Between the Ti_2AlC MAX-phase and $TiAl_2$ layer a few Nb- and Cr-rich precipitates were observed, which could not be identify within this study because of their small grain sizes. Below the Al-rich layer of $TiAl_2$, the nominal chemical composition of the TiAl-48-2-2 substrate material was measured. An outward diffusion of niobium from the substrate material into the Cr–Al–C coating was not observed. A formation of Cr_2O_3 or TiO_2 was detected neither on top of, nor in the coating, nor in the IDZ. At the interface between Cr–Al–C coating and alumina layer some small horizontal cracks formed, indicating the beginning delamination of the coating material on the TiAl48-2-2 material, although no macroscopic spallation was observed.

The XRD measurement at room temperature after the high temperature exposure for 100 h at 800 °C (see **Figure 8**) confirm the formation of hexagonal Cr_2AlC, orthorhombic Cr_7C_3, as well

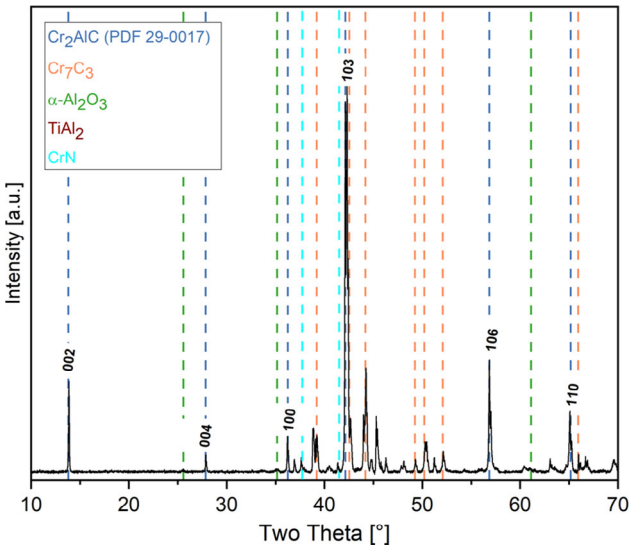

Figure 8. Room temperature XRD difractograms of the Cr–Al–C coating on TiAl48-2-2 alloy after 100 h of exposure to 800 °C in laboratory air.

as cubic CrN. Ti_2AlC in the IDZ could not be detected by the XRD, because the X-ray penetration depth at the corresponding angles was not sufficient.

3.3.2. Application of the Ti–Al–C Coating on the TiAl48-2-2 Alloy

Figure 9 shows the SEM cross section of the Ti–Al–C-coated TiAl48-2-2 alloy after isothermal exposure to 850 °C for 300 h in lab air. The chemical composition measured by EDS in at % is shown in **Table 5**.

The Ti–Al–C coating developed a homogeneous binary Ti_2AlC MAX-phase below a 1 µm thin TGO layer of pure alumina on the coating surface. In contrast to the Ti–Al–C-coated Al_2O_3 substrates, the formation of an outer thermally grown TiO_2 layer above the alumina layer could not be observed. By comparing with the nominal chemical composition of the coating after the deposition process (Figure 4), an outward diffusion of

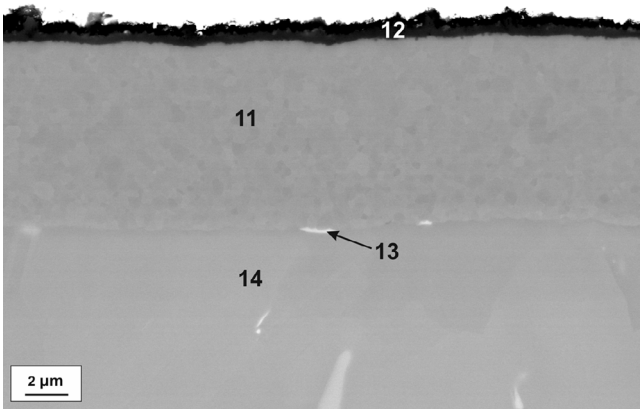

Figure 9. SEM cross section of the Ti–Al–C coating after isothermal exposure of 300 h to 850 °C in air with the nominal chemical composition using EDS in at%.

Table 5. Chemical composition of the spots 11–14 shown in Figure 9, measured by EDS in at%.

Concentration [at%]	Ti	Al	C	O	Cr	Nb
11 Ti_2AlC MAX-phase	57	24	19	–	–	–
12 TGO of Al_2O_3	6	31	–	63	–	–
13 Cr-rich precipitates	44	35	9	–	10	2
14 TiAl48-2-2 substrate	48	44	–	4	2	2

titanium from the substrate into the coating and a carbon inward diffusion into the substrate occurs, whereas the Al content stays more or less constant (see spot 11 in Table 5).

At the coating/substrate interface, few small Nb- and Cr-rich precipitates were formed similar to the IDZ on the Cr–Al–C-coated TiAl48-2-2 alloy. Further carbide or nitride formation based on titanium like TiC or TiN could not observed in the Ti–Al–C coating, the sputter coating EDS results indicate a homogenous composition, which corresponds to the binary Ti_2AlC MAX-phase. The initial columnar coating morphology was not visible anymore after high temperature exposure similar to the coated Al_2O_3 substrates. Below the Ti–Al–C coating, the EDS measurements confirm the composition of the TiAl48-2-2 substrate material, no IDZ is visible in the cross section. An outward diffusion of niobium from the TiAl48-2-2 substrate into the Ti–Al–C coating could also not be detected.

A section of the XRD results from 10° to 65° after exposure to 850 °C up to 300 h is shown in **Figure 10** and confirms the formation of the binary Ti_2AlC MAX-phase. The *hkl*-indexes of the Ti_2AlC pattern are inserted. The further reflections belong to α-Al_2O_3, TiO_2, and γ-TiAl (substrate) and were neglected for a better overview of the diffractogram.

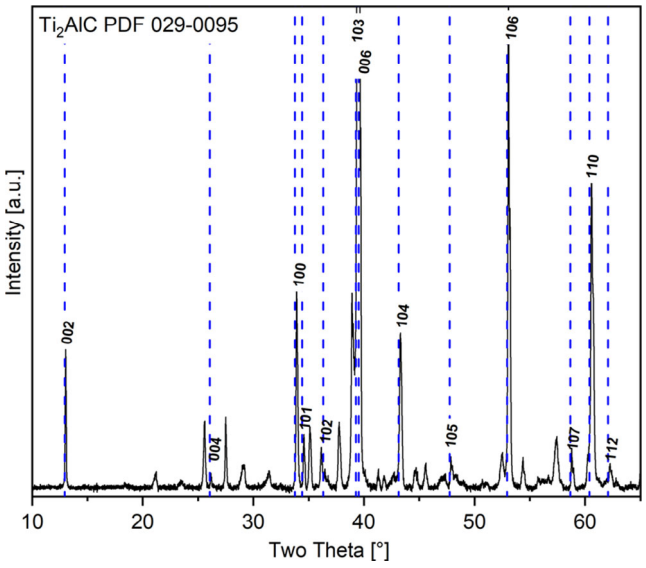

Figure 10. Room temperature XRD diffractogram of the Ti–Al–C coating on TiAl48-2-2 alloy after 300 h of exposure to 850 °C in laboratory air.

4. Discussion

4.1. Deposition and Phase Formation of the MAX-Phase Forming Cr–Al–C and Ti–Al–C Coatings on Al_2O_3 Substrates

The deposition of the MAX-phase forming 49Cr–27Al–24C as well as 41Ti–26Al–33C (in at%) coating by DC magnetron sputtering using four pure elemental targets was successfully demonstrated. In comparison with previous work by Stelzer et al.[37] the coating deposition rate could be significantly increased using two carbon sources, as well as a pure Al and Cr or Ti target. Therefore, an initial coating thickness of more than 7 µm was achieved after the sputter process. An enhancement of the layer growth rate, which is limited due to the low sputter rate of carbon, is essential for future planned applications as material for protective coatings in high temperature environments to increase economic viability. Moreover, the utilization of pure elemental targets enables a simple adjustment of each target power to compensate the varying sputter yields of the different elements in comparison with the utilization of a compound targets. Furthermore, process control is easier and the utilization of solid carbon targets is a clean solution in comparison with reactive sputtering processes with gaseous hydrogen carbons.

An isothermal heat treatment in laboratory air up to 1000 °C with in situ HT-XRD measurements reveals the formation of the desired hexagonal MAX-phases of Cr_2AlC or Ti_3AlC_2 with protective thermally grown oxide layers on top on the Al_2O_3 substrate material. Consequently, it is found that a postcoating heat treatment must not necessarily be done under inert conditions (e.g., under vacuum or protective atmospheres) for the development of the required MAX-phase, i.e., annealing in air is sufficient to create the desired phases prior to the exposure of the investigated coatings to high temperature environments. The oxidation protection is sufficient using amorphous sputter coatings that start to form the desired MAX-phases when used in high temperature applications and simultaneously develop the protective TGO.

The in situ HT-XRD measurements reveal the formation of the binary Cr_2AlC MAX-phase at a temperature of 600 °C and the development of the ternary Ti_3AlC_3 MAX-phase at 700 °C in air, which is in agreement with previous work.[33,37] The higher self-adjusted substrate temperature (see Table 1) during the Cr–Al–C deposition process in comparison with the Ti–Al–C deposition process could already be an indicator for the development of molecular compounds during the magnetron sputter process. For future applications of these MAX-phase forming coatings, a production process noticeably below the service temperature of the used high temperature alloy is required to prevent any negative influence of coating heat treatment on the microstructure and thus the mechanical properties of the substrate material. Therefore, the application of these sputter coatings for γ-TiAl-based substrates, which were commonly used at about 750 °C, is conceivable.

The initially formed columnar structure is in accordance with zone 1 by the structure zone model by Thornton[36] due to the T_s/T_m ratios of about 0.134 for the deposition of the Cr–Al–C coating and 0.116 for the Ti–Al–C coating (calculated with the melting temperatures of Cr and Ti, respectively). The lower melting point of titanium in comparison with chromium leads to a

higher mobility of titanium during the sputtering process, which leads to smaller intercolumnar gaps and finally to a higher coating density already after the deposition process. Moreover, the initial formed coating gaps disappear during the high temperature exposure due to the enhanced diffusion of titanium in comparison with chromium. Therefore, the Ti–Al–C coating develops a homogenous, dense morphology even at lower temperatures before any oxidation processes like the formation of alumina starts.[38] In comparison, the Cr–Al–C coating retained the initial formed columnar morphology after exposure to 1000 °C in air. The coating gaps are filled with alumina, confirming the known "self-healing effect" of these MAX-phase-based coatings.[39,40] For future-planned applications, a good protection against oxidation seems suitable but the promising mechanical properties of the MAX-phases could be reduced due to internal alumina formation within the column gaps.

The Cr_2AlC MAX-phase-based coating developed a TGO of α-Al_2O_3 on the surface on alumina substrates, which provides the required diffusion controlled slow parabolic growth rate during high temperature exposure. No Cr_2O_3 formation was detected by HT–XRD confirming the preferential oxidation of Al from the Cr_2AlC MAX-phase due to the stronger, covalent Cr—C bonding and the weaker, metallic Cr—Al bonding in the Cr_2AlC MAX-phase.[41] However, the formation of the $Cr_{23}C_6$ phase was also observed up to a temperature of 700 °C, although the initially precise stoichiometric chemical composition of 49Cr–27Al–24C (in at%) was measured by WDS. The alumina formation leads to a depletion of Al in the coating and simultaneously to a surplus of Cr and C, which results in the formation of the chromium carbides and the dissolution of the Cr_2AlC MAX-phase until 800 °C. In this work, the $Cr_{23}C_6$ phase was observed on the Cr–Al–C-coated alumina substrates, whereas on the later discussed TiAl48-2-2-based substrate, the formation of the Cr_7C_3 phase with a lower carbon content was detected by XRD as well as EDS element mappings. The reason for the development of this metastable $Cr_{23}C_6$ phase on alumina substrates with a lower C-content of ≈21 at% (vs 30 at% in Cr_7C_3) is yet not clear. Differences in the initial chemical coating composition can be excluded, because all Cr–Al–C-coated samples were coated in the same deposition run. On the TiAl48-2-2 substrate, the Cr_7C_3 phase formed, although the observed inward diffusion of carbon into the TiAl48-2-2 substrate, which is in accordance with previous work by Gonzalez-Julian et al., on Cr_2AlC-coated Ni-based alloy.[17]

The ternary Ti_3AlC_2 MAX-phase formed on the alumina substrates developed a TGO dual layer, consisting of an upper TiO_2 layer and an underlaying Al_2O_3 layer, which is in agreement with previous work.[42] Due to the lower Al content of 17 at% in the ternary MAX-phase, the initial oxidation process starts with the formation of a TiO_2 layer, at further oxidation also the formation of α-Al_2O_3 could be observed.[42] Although TiO_2 is not able to protect against oxygen inward diffusion, the underlaying formed continuous and dense alumina layer seems sufficient as an oxidation protection layer. Moreover, the ability of the Ti_3AlC_2 MAX-phase to form Al_2TiO_5 at temperatures above 1200 °C could be suitable by the utilization as an environmental barrier coating due to a good resistance against water vapor.[43] The formation of Ti–C could not be observed in the Ti–Al–C coating, probably because of the initial oxidation of Ti and therefore a resulting minor Al depletion and surplus of titanium. The ternary Ti_3AlC_2 phase shows a thermodynamically stable formation below the TGO on the alumina substrates and no other carbide or nitride phases confirming a beginning dissolution of the MAX-phase that could be observed after exposure to 1000 °C in air. However, future planned TEM investigations are necessary for a clear-phase identification.

4.2. Deposition and Phase Formations of the MAX-Phase Forming Coatings on the γ-TiAl-Based Alloy TiAl-48-2-2

The deposition of homogenous all-around coatings on flat coupon samples made of TiAl48-2-2 was successfully demonstrated with a coating thickness of around 7 μm for both coatings. The SEM cross sections of the Cr–Al–C coating as well as of the Ti–Al–C coating show a similarly good adhesion on the TiAl-48-2-2 substrate material like on the alumina substrates after the deposition process in the as-coated state. During the isothermal high temperature exposure in laboratory air, no visible spallation was observed, although the CTE of the formed Cr_2AlC MAX-phase with 13×10^{-6} (K^{-1}) is significantly higher than that of the TiAl-based substrate material with about 10×10^{-6} (K^{-1}).

Surprisingly, the SEM cross-sectional analysis reveals that no formation of a TGO layer on the Cr–Al–C coating surface occurred. After 100 h at 800 °C, large parts of the Cr_2AlC phase MAX-phase were already dissolved and the Cr_3C_7 as well as the CrN phase formed next to internal oxidation of Al to alumina in the coating. The internal oxidation of the coating is caused by the columnar structure of the sputter coating. Probably, postheat treatment of the Cr–Al–C layer in a high vacuum atmosphere could lead to a more compact coating microstructure and therefore to less internal oxidation by a reduced oxygen diffusion along the intercolumnar surfaces. Instead of a TGO on the coating surface, a homogenous alumina layer at the interface between coating and substrate was formed providing at least an initial oxidation protection of the TiAl substrate material. Due to the inward diffusion of C into the TiAl substrate, the formation of an IDZ occurs, consisting of the binary Ti_2AlC MAX-phase with an underlaying $TiAl_2$ layer. It is assumed that the formation of the alumina layer at the coating–substrate interface occurs due to the oxidation of this Ti_2AlC MAX-phase at the substrate surface. Horizontal cracks between Cr–Al–C coating and TiAl substrate were observed by SEM after 100 h of exposure to 800 °C in lab air. This is probably caused by mismatches in the CTE's between Ti_2AlC MAX-phase and the chromium nitride and carbide phases above it. Below this Ti_2AlC MAX-phase layer, the formation of an Al-rich layer of probably the $TiAl_2$ phase was evident to compensate the higher Al content originating from the loss of Ti, which is in turn caused by the formation of the Ti_2AlC phase. Abdulkadhim et al. have already suggested the high thermodynamic stability of the Ti_2AlC phase in the presence of the γ-TiAl phase, which would explain the appearance of this MAX-phase in the IDZ of the Cr–Al–C-coated TiAl48-2-2 alloy.[33]

The Ti–Al–C coating provides an excellent oxidation protection for the TiAl48-2-2 substrate material up to 850 °C for 300 h due to the development of a TGO from pure alumina on the coating surface. In contrast to the Ti–Al–C-coated alumina substrates, the binary MAX-phase Ti_2AlC was formed on the

TiAl48-2-2 alloy. The XRD measurements shown in Figure 10, the homogenous TiAl ratio of 2:1 and the absence of an outer TiO_2 layer as part of the TGO confirm the development of this binary MAX-phase. The Ti–Al–C coating/substrate interface is marked by a few small C- and Cr-rich precipitates that have formed most likely by a minor solution of C in the TiAl substrate material. Further TEM investigations are necessary to identify these precipitates, which goes beyond the scope of this investigation. The formation of an IDZ like the one found on the Cr–Al–C-coated TiAl48-2-2 sample could be avoided, indicating less interdiffusion between Ti–Al–C coating and TiAl48-2-2 substrate material. Different previous have already shown that γ-TiAl promotes the formation of the hexagonal binary Ti_2AlC MAX-phase.[33] In the presence of the γ-phase, the Ti_2AlC is thermodynamically more stable than the TiC phase, which was already published by Lee et al. Furthermore, theoretical thermodynamically calculations by Mitra et al. confirm this finding.[44,45] Finally, an excellent adhesion of the Ti–Al–C coating was given due to similar CTE's of the developed binary Ti_2AlC MAX-phase and the TiAl48-2-2 substrate material providing a high potential of such Ti-based MAX-phase forming coatings as protective layers for γ-TiAl-based alloys.

It can be concluded that the substrate-dependent behavior of the MAX-phase-based coatings is dominated by interdiffusion processes. On the inert alumina substrates, no interdiffusion between coating and substrate could be observed and therefore the substrate-independent performance of the coating at high temperature exposure could be analyzed. In contrast, the TiAl48-2-2 sample showed significant interdiffusion processes especially in case of the Cr–Al–C coating. This is one main driving force causing the dissolution of the Cr_2AlC MAX-phase on TiAl leading to a failure of the coating. As expected, the Ti–Al–C coating developed the binary Ti_2AlC MAX phase due to Al outward diffusion from the Al-richer TiAl48-2-2 substrate into the coating.

5. Conclusions

In summary, the sputtered Cr–Al–C as well as the Ti–Al–C coating are promising as protective layers for high temperature applications due to the development of MAX-phases, which have the ability to form protective TGO layers. The performance of the MAX-phases during high temperature exposure is strongly dependent on the substrate material that influences interdiffusion processes and thus the evolution of phases during high temperature exposure. The key issues of the present work are summarized as followed: 1) The deposition of MAX-phase forming Cr–Al–C and Ti–Al–C coatings in an industrial-sized multi-source magnetron sputter machine using four pure elemental targets was successfully demonstrated with a received coating thickness of >7 µm. 2) Homogenous all-around deposition of the coatings on the alloy TiAl48-2-2 with sufficient adhesion during 300 h high temperature exposure in the temperature range between 800 and 850 °C was proven. 3) The Ti_2AlC MAX-phase formation from amorphous coatings with simultaneously development of protective thermally grown oxide layers by annealing in air is sufficient and can replace an additional postheat treatment in inert atmospheres. 4) The Cr_2AlC MAX-phase is thermodynamically not stable on the TiAl48-2-2 alloy and disintegrates into different carbide and nitride phases. A protective TGO on top of the coating was not established, instead an internal alumina layer has formed between coating and TiAl. 5) The ternary Ti_3AlC_2 on alumina substrate as well as the binary Ti_2AlC MAX-phase on the TiAl48-2-2 alloy provide a strong thermodynamic stability and therefore an excellent oxidation behavior due to the development of slow growing and protective TGO layers. 6) Especially, the binary Ti_2AlC MAX-phase is promising for future applications on γ-based titanium aluminides due to the good thermodynamic compatibility in the presence of the γ-TiAl phase.

Acknowledgements

The authors thank Mr. Jörg Brien for coating manufacturing using DC magnetron sputtering as well as Ms. Lisa Klamann for her support in preparing the metallographically cross sections for the SEM analysis. Furthermore, the authors thank Prof. Dr. Uwe Schulz for helpful comments and the proof reading.

Open access funding enabled and organized by Projekt DEAL.

Conflict of Interest

The authors declare no conflict of interest.

Data Availability Statement

Research data are not shared.

Keywords

Cr_2AlC, DC magnetron sputtering, oxidation protective coatings, Ti_2AlC and Ti_3AlC_2 MAX-phase, γ-based titanium aluminides

Received: June 9, 2021
Revised: July 16, 2021
Published online:

[1] P. Eklund, M. Beckers, U. Jansson, H. Högberg, L. Hultman, *Thin Solid Films* **2010**, *518*, 1851.
[2] Z. M. Sun, *Int. Mater. Rev.* **2011**, *56*, 143.
[3] M. Radovic, M. W. Barsoum, *Bulletin* **2013**, *92*, 20.
[4] G. Deysher, C. E. Shuck, K. Hantanasirisakul, N. C. Frey, A. C. Foucher, K. Maleski, A. Sarycheva, V. B. Shenoy, E. A. Stach, B. Anasori, Y. Gogotsi, *ACS Nano* **2020**, *14*, 204.
[5] J.J.O.O.M. Smialek, *Oxidat. Met.* **2015**, *83*, 351.
[6] A. G. James Smialek, Harder Bryan, Nesbitt James, Gabb Timothy, Gray Simon, in *Oxidation of Alumina-Forming MAX Phases in Turbine Environments, Nasa Technical Report*, **2017**, https://core.ac.uk/reader/80604550.
[7] J. L. Smialek, *Metall. Mater. Trans. A* **2018**, *49*, 782.
[8] F. Zhang, S. Yan, C. Li, Y. Ding, J. He, F.J.J.O.T.E.C.S. Yin, *J. Eur. Ceram. Soc.* **2019**, *39*(16), 5132.
[9] M. W. Qureshi, X. Ma, G. Tang, B. Miao, J. J. M. Niu, *Materials* **2021**, *14*(4), 826.
[10] H. Rueß, J. Werner, Y. Unutulmazsoy, J.W. Gerlach, X. Chen, B. Stelzer, D. Music, S. Kolozsvari, P. Polcik, T.E.J.J.O.T.E.C.S. Weirich, *J. Eur. Ceram. Soc. 41*(3), (**2021**) 1841-.

[11] H. Yeom, B. Hauch, G. Cao, B. Garcia-Diaz, M. Martinez-Rodriguez, H. Colon-Mercado, L. Olson, K.J.T.S.F. Sridharan, *Thin Solid Films* **2016**, *615*, 202.
[12] Z. Feng, P. Ke, Q. Huang, A. J. S. Wang, C. Technology, *Surf. Coat. Technol.* **2015**, *272*, 380.
[13] O. Berger, R. Boucher, *Surf. Eng.* **2017**, *33*, 192.
[14] W. Garkas, M. Fröhlich, K.-D. Weltmann, C. Leyens, *Mater. Sci. Forum* **2015**, *825–826*, 628.
[15] W. Garkas, C. Leyens, A. Flores-Renteria, *Adv. Mater. Res.* **2010**, *53*, 208.
[16] O. Schroeter, *Holzforschung* **2011**, *40*, 51.
[17] J. Gonzalez-Julian, G. Mauer, D. Sebold, D. E. Mack, R. Vassen, *J. Am. Ceram. Soc.* **2020**, *103*, 2362.
[18] N. Laska, R. Braun, S. Knittel, *Surf. Coat. Technol.* **2018**, *349*, 347.
[19] M. P. Brady, J. L. Smialek, J. Smith, D. L. Humphrey, *Acta Mater.* **1997**, *45*, 2357.
[20] R. Braun, K. Kelm, M. Fröhlich, C. Leyens, *Surf. Coat. Technol.* **2013**, *222*, 128.
[21] V. Gauthier, F. Dettenwanger, M. Schütze, V. Shemet, W. J. Quadakkers, *Oxidat. Met.* **2003**, *59*, 233.
[22] A. Knaislová, P. Novák, M. Cabibbo, L. Jaworska, D. Vojtěch, *Review* **2021**, *14*, 1030.
[23] R. Swadźba, L. Swadźba, B. Mendala, P.-P. Bauer, N. Laska, U. Schulz, *Surf. Coat. Technol.* **2020**, *403*, 126361.
[24] P.-P. Bauer, N. Laska, R. J. I. Swadźba, *Intermetallics* **2021**, *133*, 107177.
[25] N. Laska, R. Braun, *Mater. High Temp.* **2015**, *32*, 221.
[26] R. Braun, N. Laska, S. Knittel, U. Schulz, *Mater. Sci. Eng. A* **2017**, *699*, 118.
[27] M. W. Barsoum, M. Radovic, *Annu. Rev. Mater. Res.* **2011**, *41*, 195.
[28] S. Gupta, M. J. W. Barsoum, *Wear* **2011**, *271*, 1878.
[29] M. Barsoum, T. El-Raghy, M. J. M. Ali, *Metall. Mater. Trans. A* **2000**, *31*, 1857-1865.
[30] P. Bartolotta, J. Barrett, T. Kelly, R. J. J. Smashey, *JOM* **1997**, *49*, 48-50.
[31] W.-B. Tian, P.-L. Wang, G.-J. Zhang, Y.-M. Kan, Y.-X. Li, *J. Am. Ceram. Soc.* **2007**, *90*, 1663.
[32] A. Abdulkadhim, M. Baben, T. Takahashi, V. Schnabel, M. Hans, C. Polzer, P. Polcik, J.M.J.S. Schneider, *Surf. Coat. Technol.* **2011**, *206*, 599.
[33] A. Abdulkadhim, T. Takahashi, D. Music, F. Munnik, J.M.J.A.M. Schneider, *Acta Mater.* **2011**, *59*, 6168.
[34] Q. Wang, A. F. Renteria, O. Schroeter, R. Mykhaylonka, C. Leyens, W. Garkas, *Surf. Coat. Technol.* **2010**, *204*, 2343.
[35] M. C. Galetz, A. S. Ulrich, C. Oskay, D. Fähsing, N. Laska, U. Schulz, M. Schütze, *Intermetallics* **2020**, *123*, 106830.
[36] J. A. Thornton, *J. Vac. Sci. Technol. A: Vac. Surf. Films* **1986**, *4*, 3059.
[37] B. Stelzer, X. Chen, P. Bliem, M. Hans, B. Völker, R. Sahu, C. Scheu, D. Primetzhofer, J.M.J.S.R. Schneider, *Sci. Rep.* **2019**, *9*, 1.
[38] B. A. Movchan, A. V. Demchishin, *Fiz. Metal. Metalloved* **1969**, *28*, 653.
[39] S. Li, G. Song, K. Kwakernaak, S. van der Zwaag, *J. Eur. Ceram. Soc.* **2012**, *32*, 1813.
[40] O. Berger, C. Leyens, S. Heinze, M. To Baben, J. Schneider, in *Proc. of the 4th Int. Conf. on Self-Healing Materials*, Ghent University; Delft University of Technology, Ghent, Belgium **2013**.
[41] M. W. Barsoum, *MAX Phases: Properties of Machinable Ternary Carbides and Nitrides*, Wiley-VCH Verlag GmbH & Co. KGaA, Weinheim, Germany **2013**.
[42] X. Wang, Y. J. C. S. Zhou, *Corrosion Sci.* **2003**, *45*, 891.
[43] J.J.J.O.T.C.S.O.J. D. Doni, *J. Ceram. Soc. Jpn.* **2003**, *111*, 860.
[44] K. Lee, H. Sim, H. J. M. Kwon, *Metall. Mater. Trans. A* **2005**, *36*, 2517.
[45] R. Mitra, W. Chiou, J. Weertman, M. Fine, R. Aikin, *MRS Proc.* **1991**, *238*, 871.